A ROM BASED FLUTTER PREDICTION PROCESS AND ITS VALIDATION WITH A NEW REFERENCE MODEL

R. Voss, L. Tichy, R. Thormann

DLR Institute of Aeroelasticity
Bunsenstraße 10, 37073 Göttingen, Germany
Ralph.voss@dlr.de, Lorenz.tichy@dlr.de, Reik.thormann@dlr.de

Keywords: transonic flutter, ROM, aeroelastic test cases, unsteady aerodynamics, flutter computation process

Abstract: Industrial flutter prediction for large transport aircraft requires numerical capabilities to predict unsteady aerodynamic forces induced by harmonic oscillations for the complete flight envelope including transonic and separated flow conditions, with shock boundary layer interaction and inverse shock motion.
Adequate numerical methods have to model both flow physical and geometrical complexities in more detail than the standard DLM approach. The application of CFD methods results in a more or less time consuming task. On the other hand the aircraft development process, which leads to structural modifications with impact on the flutter behaviour, requires robust and accurate analyses for various stiffness and/or mass conditions in short iteration times.
Thus the CFD calculation process should be decoupled from the structural analysis process. This can be achieved by application of aerodynamic reduced order models (ROM). A new method following this strategy is presented. It relies on a limited number of unsteady CFD computations forming the ROM data base, combined with an arbitrary number of Doublet Lattice computations. Thus compatibility with standard DLM based linear flutter prediction process is conserved. The quality of the new approach depends significantly on the choice and number of single CFD computations, as well as on mapping of these results to the DLM aerodynamic data structure.
The validation of this approach is performed in a first step by comparing unsteady pressure distributions and generalised airloads for cases of the parameter space, which have not been included in the data base. In a second step the complete process validation requires a common aeroelastic reference test case of adequate complexity. A brief review of available windtunnel data for both unsteady aerodynamics and flutter outlines the shortcomings of these data, like missing measurements of a clear transonic dip significantly below Mach number one, and of inverse shock motions.

A new common test configuration with a transonic dip flutter boundary in the Mach number range between 0.80 and 0.95 is proposed. The aircraft geometry from the Drag-Prediction Workshop 4 fulfils the above mentioned unsteady aerodynamic requirements. It is extended to a flutter model of a generic aircraft. The capability of this model is demonstrated by applying the above flutter process. An unsteady aerodynamic ROM is generated in the 3 dimensional parameter space of Mach number, reduced frequency and elastic mode shape. For selected points of this parameter space a sufficient number of unsteady RANS simulations is performed to display unsteady pressure distributions at Mach numbers between 0.6 and 0.90, and reduced frequencies up to 4. A constant lift coefficient of 0.50 has been chosen for all Mach numbers. DLR's TAU code is applied for attached flow conditions in linear modus. The ROM is completed by performing this procedure for several so called synthetic modes, which are chosen properly to display all realistic structural modes (of the fixed aircraft geometry), without their detailed knowledge.

1 INTRODUCTION

Unsteady CFD simulations have meanwhile been validated for various reference configurations, like the AGARD standard configurations, among them the LANN wing with a double shock system [1], or the Aerostabil wing with modern supercritical wing geometry [2], and recently the HIRENASD wing with high Reynolds numbers [3, 4].
Full aircraft configurations are not available. Results are encouraging although not all problems of unsteady flow separation and grid convergence have yet been solved. A typical characteristic of unsteady transonic aerodynamics is the appearance of so-called inverse shock motion, induced by shock-boundary-layer separation. This has been observed already in the early LANN wing tests, see figure 1. Comparing two transonic test cases with oscillating shocks for attached or partly separated mean flow are showing unsteady pressure peaks of different signs. It is likely that this sign change causes the ascending part of the transonic dip flutter boundary.

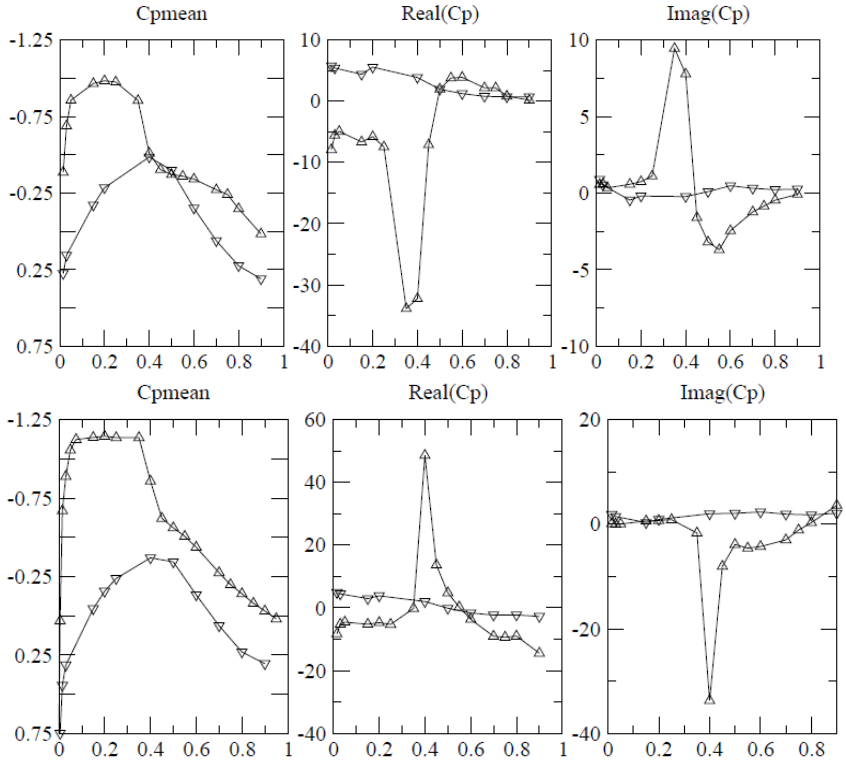

Figure 1: unsteady Cp distribution for pitching LANN wing at 47.5% span position
Upper: CT5: Ma=0.820, α = 0.60 deg, attached flow; Lower: CT9: Ma=0.820, α = 2.60 deg, separated flow

In contrast to unsteady aerodynamic data for forced harmonic motion there is an important demand in a common aeroelastic model with significant geometrical, structural and aerodynamic complexity. A few open test case models like the AGARD445.6 wing [5], Goland wing [6], Aerostabil wing [2] and MDO wing [7] are used frequently, but they lack mainly in geometrical complexity. The Goland and AGARD445.6 wings are not representative for modern transport aircraft due to their very thin and conventional profile shapes and non-tapered planforms. Their flutter boundaries exhibit a transonic dip close to Mach number one, and are hardly influenced by viscous effects or flow separation. The Aerostabil wing is rather a representative test case, but only LCO results are available. A

typical flutter boundary of a modern transport aircraft exhibits a transonic dip, which looks like figure 2. Some examples of flutter boundaries from windtunnel tests and from corresponding numerical simulations may be found for the supercritical NLR7301 airfoil and for the AMP wing in [8, 9].

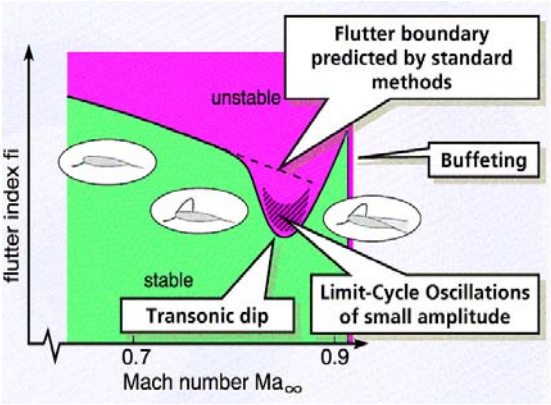

Figure 2: typical transonic dip flutter boundary

Various flutter computation assessments for more complex configurations have been reported in the literature, but they are based on proprietary models, for example the Fokker model [10], AMP [11] and Mavric [12]. The restricted availability of the most interesting models is natural because these windtunnel tests were very expensive.

On the other hand reduced order models (ROM) are developed, which will soon make the immense task of CFD based flutter simulations for complete flight envelopes feasible. These methods are mainly demonstrated for the above mentioned simplified generic open model wings, thus not enabling a realistic demonstration of the capabilities of aeroelastic ROMs. For this reason we propose a common numerical model which meets the mentioned requirements, and to apply numerical methods for flutter prediction to this test case. Usually the validation of the aerodynamic part of a numerical flutter method can be sufficiently achieved by unsteady aerodynamic windtunnel tests for forced model oscillations. But complete flight envelopes of modern transport aircraft with their immense number of parameter combinations can not be treated by straightforward application of CFD aerodynamics, neither via time-domain fluid structure coupling (CFD-CSM) nor by a standard process in the frequency domain. The latter requires many thousands of unsteady CFD simulations for all relevant combinations of Mach numbers, load cases, reduced frequencies, and structural mode shapes. The former is only able to provide frequency and damping values for one chosen point in the flight envelope. This situation is often complicated by the fact that the final structural dynamic model is only provided in a very late stage of the aircraft development process. This is probably one reason why flutter computation for large transport aircraft until now still relies on strategies adopting the more than 40 years old aerodynamic Doublet Lattice method [13]. The advantages of these strategies are twofold: a rapid and user-friendly unsteady aerodynamic method and the separation of unsteady airload calculation and flutter analysis. Thus it seems to be most promising to adopt high-end CFD simulations while retaining the mentioned advantages in order to design new flutter computation methods which promise the same precision for transonic and viscous flow as the old methods do for subsonic flow.

Much promising work has been performed in this direction during the last 20 years. First these efforts addressed the aerodynamic part of the problem alone, by development of faster unsteady CFD methods. One class of them is based on boundary-layer coupled time-domain CFD, for example the methods adopting TSD [14], Full Potential [15] or Euler [16] with

inverse boundary-layer methods or simultaneous coupling. They usually reduce the required computing times to nearly that of the corresponding inviscid code, thus providing in the case of Euler a gain of about a factor 50 in comparison to RANS. A second class is that of time-linearised frequency domain CFD, mainly for unsteady Euler and RANS equations [17]. These methods are usually about a factor of 10 faster than the full nonlinear code, but they have not yet reached maturity for separated flow. No linearised Euler-boundary layer coupled method, which might combine the savings of both classes has been developed. The optimum reduction of computing time of all these methods is thus less than 100 wrt. RANS, which is still not enough for many applications. For this reason, as a third class, correction methods for the DLM have been developed. Among them are first completely new CFD-DLM aerodynamic codes, which are an implicit extension of DLM to transonic and viscous flow, namely the TDLM [18] and iSKEM [19] codes. They need just one or two steady RANS computations as input. Secondly we have different methods of explicitly correcting DLM results by very few unsteady RANS simulations. A review of these methods which were often driven by very rough engineering approaches, is given in [20]. They are still further improved, mainly by developing proper strategies of selecting an optimal (proper minimised) number of basic points in the aerodynamics and structures parameter space for which to perform the time consuming full CFD simulations for forced motion and to interpolate between these basic results. Such methods are a prominent member of the class of so-called reduced order modelling (ROM) techniques. There is a wide spectrum of approaches for ROMs. On one hand faster CFD methods exhibit a model reduction technique themselves, and on the other hand flutter methods which treat mathematically the coupled (CFD-CSM) problem [21], are classified as ROMs too. A comprehensive overview of different methods is presented in [22]. Furthermore several combinations ROMS and reduced unsteady aerodynamic models are possible.

2 DEFINITION OF A NEW COMMON TEST CONFIGURATION

2.1 Requirements

We are looking for a configuration typical for a modern large transport aircraft, wrt geometry and structural model. Thus geometry should include wing, fuselage, tail, and engine nacelle with pylon. It should be further capable to demonstrate and assess the potential of CFD in combination with ROMs. Furthermore a large number of parameter combinations should be involved. Computation of a typical flutter boundary requires various Mach numbers, reduced frequencies, elastic modes, different load cases (steady lift, AoA, flight altitude) with corresponding static structural deformations. The test case should also include a typical transonic cruise condition as well as separated flow and inverse shock motion and thus show a transonic dip behaviour not too far from cruise Mach number and lift. The ascending part of the transonic dip should be significantly identified below Mach 1.

Due to the primary objective to validate ROM based models versus direct use of CFD, currently only method-to-method comparisons are planned which use purely theoretical structure. No additional aeroelastic wind-tunnel test is currently planned. Nevertheless, the validation of CFD methods by forced motion wind tunnel results is a precondition for the proposed ROM validation for aeroelastic test cases.

2.2 Selection of the new reference model

For this reason we propose a new common test case for assessment of flutter computation processes. Complexity of the test model has to go beyond the above mentioned existing open models. Unfortunately the geometry of only very few generic aircraft models is freely available. Some efforts in definition of common models for assessment of numerical simulations have been performed in a series of drag prediction workshops. The first three of them focused on a wing-fuselage-pylon-nacelle configuration, namely the DLR F6 model [23]. We do not take this configuration into account, because it has the disadvantage, that transonic flow exhibits significant flow separation both at the wing-fuselage junction and in the pylon-nacelle region, see fig 3. We want to avoid such flow separation effects but rather investigate shock induced separation effects on the wing.

A better suited one for our purposes seems to be the NASA model from the Drag Prediction Workshop 4 (DPW4) [24, 25]. So we started to study this model concerning its unsteady aerodynamic and flutter behaviour, adopting a generic structural model. We are using the wing-fuselage-horizontal tail geometry from the DPW4 website in form of a grid generated by DLR institute of aerodynamics and flow technology.

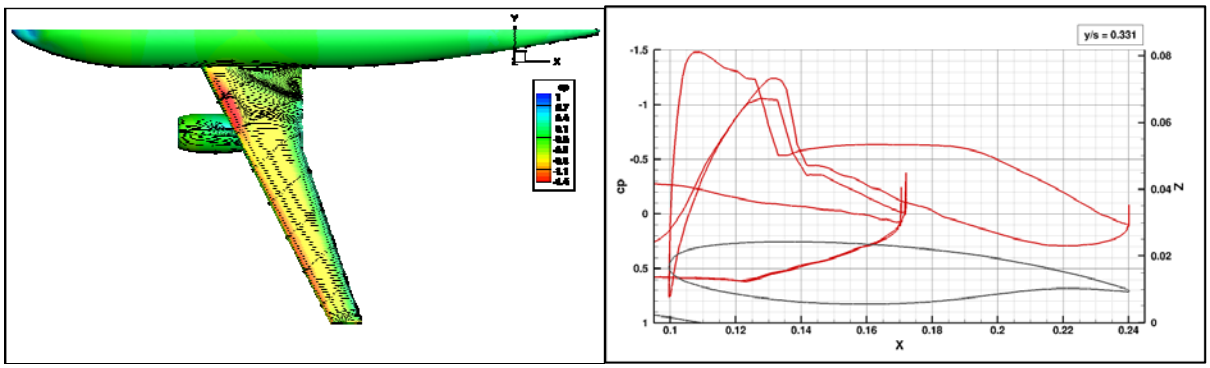

Figure 3: steady flow characteristic of the drag prediction workshop3 reference model, the DLR F6.
Left figure: skin friction lines on the surface indicating severe separation at the wing fuselage junction.
Right figure: steady pressure distribution at a spanwise station close to the nacelle, curves for the nacelle and for the lower wing indicating shock induced flow separation

First the geometrical and structural model refers to a wind tunnel model, in a second step a full aircraft model will be defined too.

2.3 Geometry

Figure 4 depicts the geometry of the windtunnel model. The reference length is root chord of the wing L=462 mm.
Currently there are no engine nacelles and pylons and no vertical tail. It is planned to complete the model later with these components.

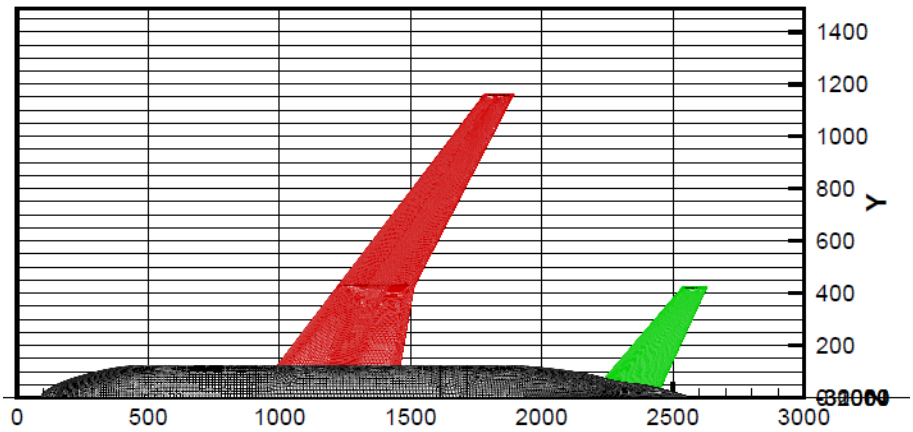

Figure 4: Geometry of the DPW4 reference aircraft model

2.4 Structure

Different models are available, namely two beam-like 6 DOFs for the wing only, see table 1, and 10 DOFs for the wing with 2 pylons and 2 nacelles. In addition a more complex FE model is available.

No	Eigenmode	Frequency [Hz]	Damping [-]	Gen. mass [kg m^2]
1	1st bending	23.39	0.0038	0.58
2	1st torsion	31.85	0.0032	10.92
3	In-plane bending	49.00	0.0114	1.63
4	2nd bending	54.99	0.0076	1.63
5	3rd bending	81.06	0.0086	5.38
6	4th bending	99.60	0.0086	5.11

Table 1: Modal properties of the reference model without engines

2.5 Aerodynamic characteristics of the reference model

Some aspects of the aerodynamics of the DPW4 model can already be studied at steady flow fields. For the reference load condition CL = 0.50 the flow becomes transonic at Ma = 0.775 and exhibits shock induced flow separation above Ma = 0.875. As a consequence we can expect regular unsteady shock motions for Ma < 0.875 and so-called inverse shock motions for Ma > 0.875. This is depicted in figures 5, 6, where the angle of attack has been once decreased by $\Delta\alpha$ = -0.25 deg and once raised by $\Delta\alpha$ = +0.25 deg around the AoA of CL = 0.50 load condition. For Ma = 0.850 the shock moves downstream with increasing α, while for Ma = 0.900 it moves upstream. This is more clearly depicted by the Cp distributions for the wing section y = 600 mm in figure 7. It should be noted, that the inverse shock motion does not alter the direction of lift change with α. The lift is still increasing with increasing AoA, because the Cp level upstream of the shock is significantly increasing, so we are still on the ascending part of the steady lift polar. But the quasi-steady derivatives of lift and moment are changing their tendency, as can be seen from figure 8.

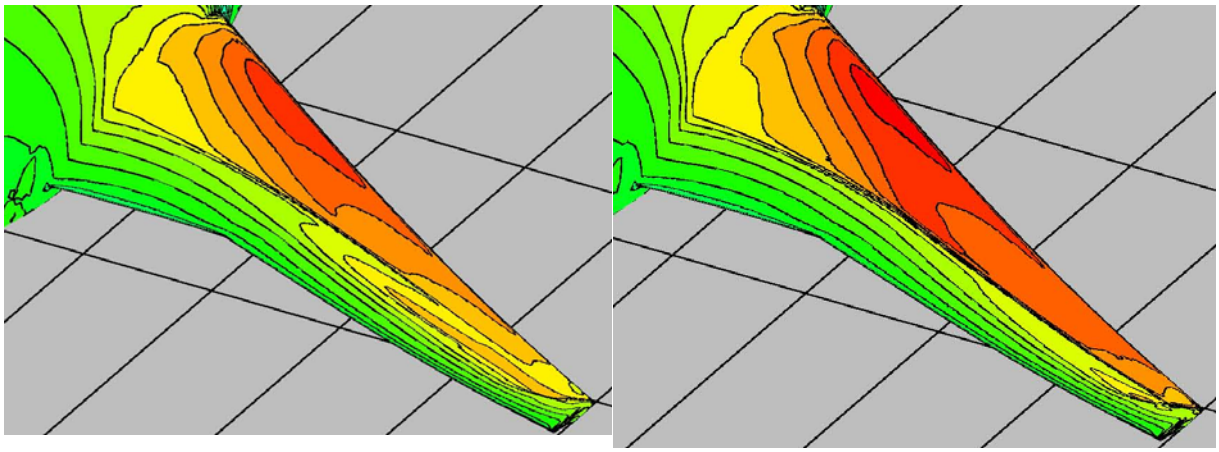

Figure 5: Ma=0.850, CL(mean)=0.50, left**:** Δα = -0.25° right**:** Δα = +0.25° → regular shock motion

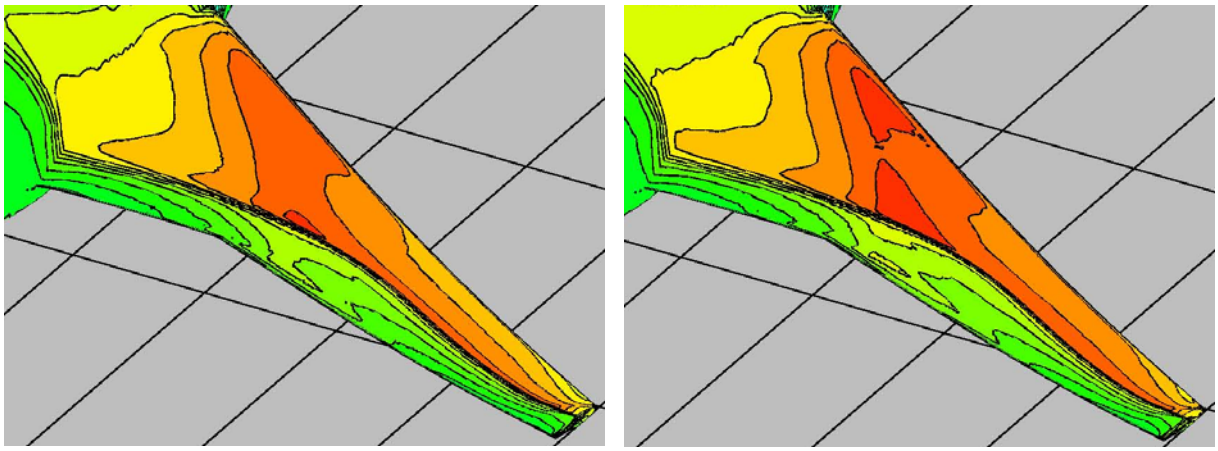

Figure 6: Ma=0.90, CL(mean)=0.50, left**:** Δα = -0.25° right**:** Δα = +0.25° → inverse shock motion

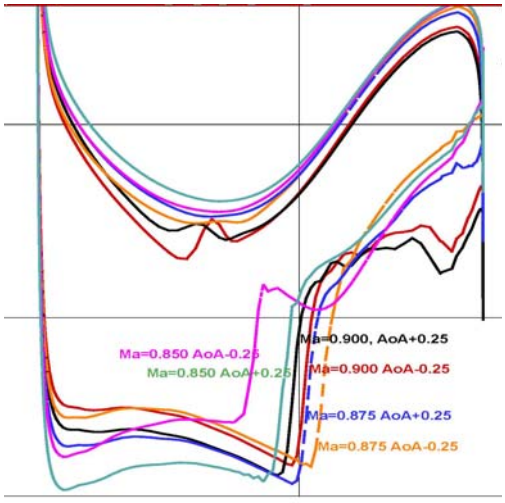

Figure 7: Chordwise Cp distributions at y=600 mm wing span position of the reference model CL(mean)=0.50

The left figure presents the steady AoA, at which the target lift of CL = 0.50 is achieved, in dependence from Mach number. There is a minimum at Ma = 0.87, which in turn means that for constant AoA, the lift curve has a maximum for this Mach number. The same holds true for the change of lift and moment due to AoA variation, extreme values are obtained for Ma = 0.86. These transonic and viscous effects are restricted to the wing, the horizontal tail does not show transonic effects up to Ma = 0.90.

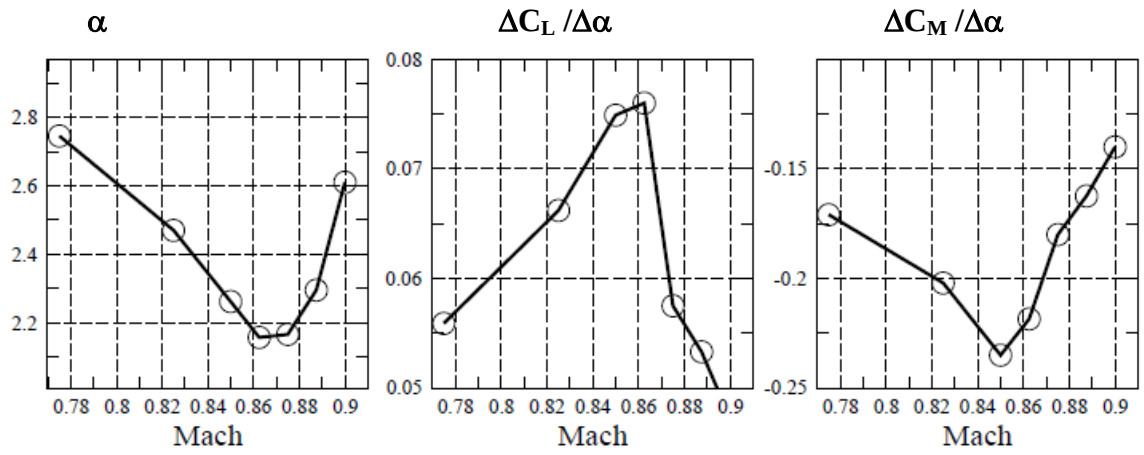

Figure 8: AoA and quasi-steady lift and moment coefficients of the reference model for CL(mean)=0.50

3 THE UNSTEADY AEORODYNAMICS REDUCED ORDER MODEL

If we want to perform a fully CFD based classical flutter computation, we will have to provide generalised unsteady airloads for all of the potentially important structural modes, for a significant number of reduced frequencies and for several Mach numbers. A fourth dimension of this parameter space would be added by taking different load cases (AoA) into account. This will result in the requirement to run about 10^5 single unsteady CFD computations for unsteady forced motions in the mode shapes of the aircraft, if we assume 10 Mach numbers, 10 reduced frequencies, 10 load cases and 100 modes. Many of these cases have to be run for transonic separated flow, which requires full Navier-Stokes simulations. In order to reduce this immense task, unsteady aerodynamic ROMs are developed. Some of them like Volterra or impulse techniques may reduce the effort in just one dimension, namely reduced frequency. Others, like Proper Orthogonal Decomposition (POD) techniques [26, 27], can help to select a more reduced number of computations, thus populating four-dimensional parameter space in a very coarse manner. Our experience shows that this strategy does not work well for the parameter axis of mode shapes. For this reason DLR elaborated a specific form of reduction technique to reduce the number of different mode shapes to be analysed by CFD, the so-called synthetic mode shape strategy.

3.1 Synthetic modes strategy

A number of *NSM* so-called synthetic mode shapes are defined:

$$\Phi_{s,n} \text{ , with: } s = 1,\ldots,NSM \qquad (1)$$

While there are *NRM* mode shapes from the structural FEM model, the so-called real modes

$$\Psi_{r,n} \text{ , with: } r = 1,\ldots,NRM \qquad (2)$$

Usually the number of synthetic modes is less than that of the structural modes: $NRM > NSM$. Both of these sets of modes are defined on the *N* boxes of a doublet-lattice grid. Unsteady DLM aerodynamic computations are performed both for all of the synthetic modes and for all of the real modes, yielding unsteady pressure distributions

$$\Delta p_{s,n}^{DLM} \quad (3)$$
$$\Delta p_{r,n}^{DLM} \quad (4)$$

Corresponding to linear frequency-domain unsteady aerodynamic theory these are complex valued first harmonics of unsteady pressure distribution induced by harmonic motion with the mode shape. Unsteady CFD computations are performed for the smaller number *NSM* of synthetic modes, yielding also unsteady complex pressure values on the *M* surface points of the CFD grid. As the CFD grid is much finer than the DLM grid, usually $M >> N$.

$$p_{s,m}^{CFD} \quad (5)$$

These results are interpolated from the CFD grid to the DLM grid, forming the corresponding pressure jumps between lower and upper lifting surfaces, which yields

$$\Delta p_{s,n}^{CFD} \quad (6)$$

Flutter computations require the corresponding results for all real modes. These are derived from the above values by the following correction process

$$\Delta p_{r,n}^{SMC} = \Delta p_{r,n}^{DLM} \cdot \sum_{s=1}^{NSM} \alpha_s \cdot F_{s,n} \quad (7)$$

This means that the final CFD corrected result, the so-called Synthetic Mode Corrected result, denoted by index SMC, is generated by multiplying the corresponding DLM result with a complex number. This number is composed as the weighted sum of the single factors

$$F_{s,n} = \Delta p_{s,n}^{CFD} / \Delta p_{s,n}^{DLM} \quad (8)$$

For each DLM grid box there is one complex valued factor per synthetic mode. The weight coefficients α_s are determined by the contribution of each synthetic mode to approximate the corresponding real mode shape. The above generation has to be performed for different Mach numbers and reduced frequency values separately.

The synthetic mode shapes have to fulfil the condition that a small number of them are sufficient to approximate all relevant real structural modes with sufficient accuracy. Different sets of synthetic mode shapes have been tested for the wing modes of a large transport aircraft structure finite element model. The first 100 Eigenmodes were taken into account by their z-deflections, only these are of relevance for the DLM based flutter process. As a measure for assessing the approximation quality the modal assurance criterion (MAC) has been adopted. The best approximation is achieved for MAC values of 100%, MAC values less than 80% denote a poor approximation. Figure 10 shows that the first 50 real modes can be sufficiently approximated (MAC > 80%) with only 10 synthetic modes. From the different candidates for synthetic mode shapes, namely simple polynomials, Legendre and Chebychev polynomials and trigonometric distributions of mode shape amplitude in wing spanwise direction, the trigonometric approach has been selected. The 10 trigonometric modes (5 bending and 5 torsional ones) are depicted in figure 9.

Applying the correction process of equations (7) and (8) for all Mach numbers, reduced frequencies and real mode shapes, the unsteady loads distribution from DLM is corrected and used for a frequency domain flutter computation.

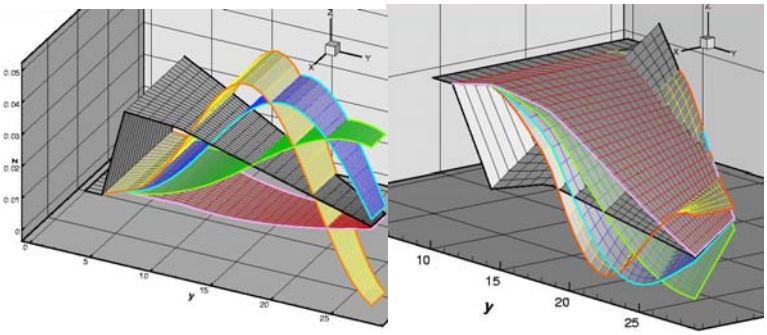

Figure 9 : Synthetic mode shapes: 5 bending, 5 pitch (right)

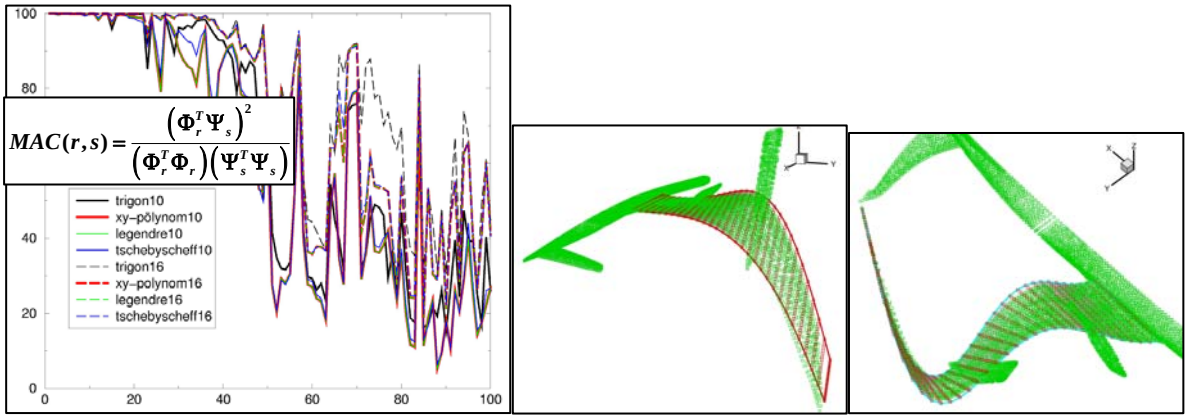

Figure 10 : Left: Approximation quality (measured as MAC value) of first 100 FEM structural mode shapes of a large transport aircraft by synthetic modes of different type and different number (10 or 16)
Right: Approximation (red) and real FEM structure mode shapes (green) of a large transport aircraft, from left to right: 7th and 22nd modes

3.2 ROM for the parameter subspace of Mach number, load cases and frequency

The synthetic mode shape strategy reduces computational efforts significantly and allows to generate the ROM data by expensive CFD simulations before the final structural model of the aircraft is available. A further reduction of the number of unsteady aerodynamic simulations cab be achieved by applying POD techniques in the remaining three-dimensional parameter sub-space of Mach number, load case and reduced frequency. This task is not part of the current paper.

3.3 CFD simulations

The unsteady aerodynamic data base with forced motion of the complete DPW4 aircraft model in the synthetic mode shapes has been generated by different CFD approaches, all of them were based on Reynolds Averaged Navier-Stokes (RANS) computations with DLR's TAU code [28,29]. The one-equation turbulence model of Spalart-Almaras [30] has been used. An unstructured CFD grid with 4 million nodes has been applied, comprising prismatic layers in regions close to the body surfaces and tetrahedral volume elements in the outer regions. The grid is depicted in figure 11. It has been created by DLR institute of aerodynamics and flow technology at Braunschweig, and may be downloaded from the DPW4 website [25].

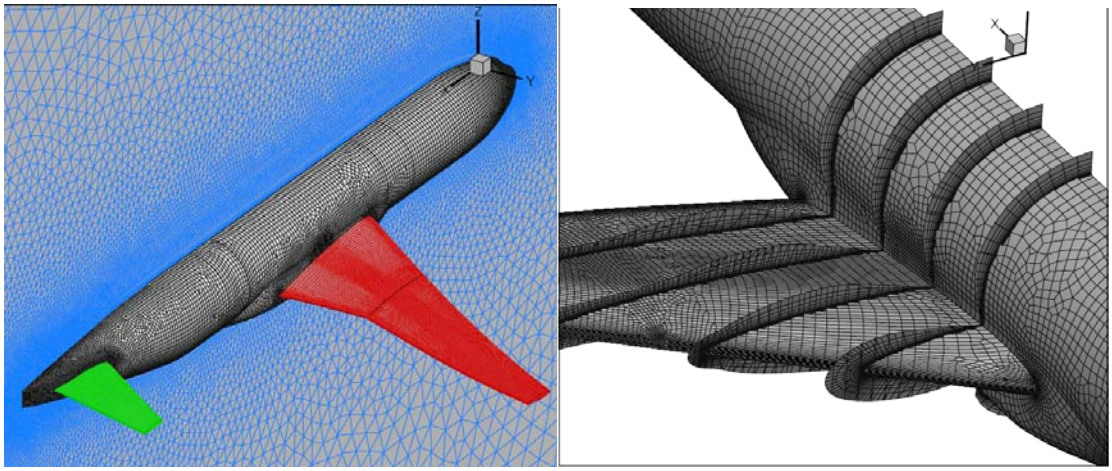

Figure 11: CFD grid of the reference model

First, steady simulations were performed for different Mach numbers and for the target lift coefficient CL = 0.50. Around the corresponding steady flow fields unsteady nonlinear simulations were performed, introducing the synthetic mode shapes as unsteady boundary condition forcing the surface structural deformations. The amplitude was chosen to be equivalent to a pitch amplitude of $\Delta\alpha$ = 0.25 degrees as the maximum value along wing span. Typically 4 oscillation cycles, each with between 256 and 512 physical time steps (depending on the reduced frequency value), were run to achieve converged periodic solutions. These time consuming simulations were performed only for the Mach numbers Ma=0.775, 0.825, 0.8625, 0.8875 and for always 3 reduced frequency values ω^* = 0.25, 0.40, 0.80. The limiting value ω^* = 0.0 has been made available by 2 steady computations with different angles of attack.

Additional computations in the Ma - ω^* parameter space will be carried out adopting faster CFD codes. For additional Mach numbers in attached flow conditions the linearised version of DLR's TAU code LFD-TAU [17] will be applied. For low reduced frequencies $\omega^* < 0.20$, the very fast iSKEM code [19] may be used both for attached and separated flows.

CFD data for ω^* = 0.0 show already a significant trend, see figure 12. The distribution of $\Delta Cp / \Delta\alpha$ on the surface indicates a significant region of large values (in red and blue colours) extending along the wing span, but of small chordwise width. This corresponds to the region where the shock wave is oscillating. With increasing Mach number, the shock moves downstream up to the most downstream location at Ma = 0.8625. With increased Mach number of 0.8875 and 0.900 the mean shock position remains nearly constant, but the sign of the unsteady shock peak changes (colour from red to blue). This is due to the before mentioned change from regular to inverse shock motion with respect to AoA.

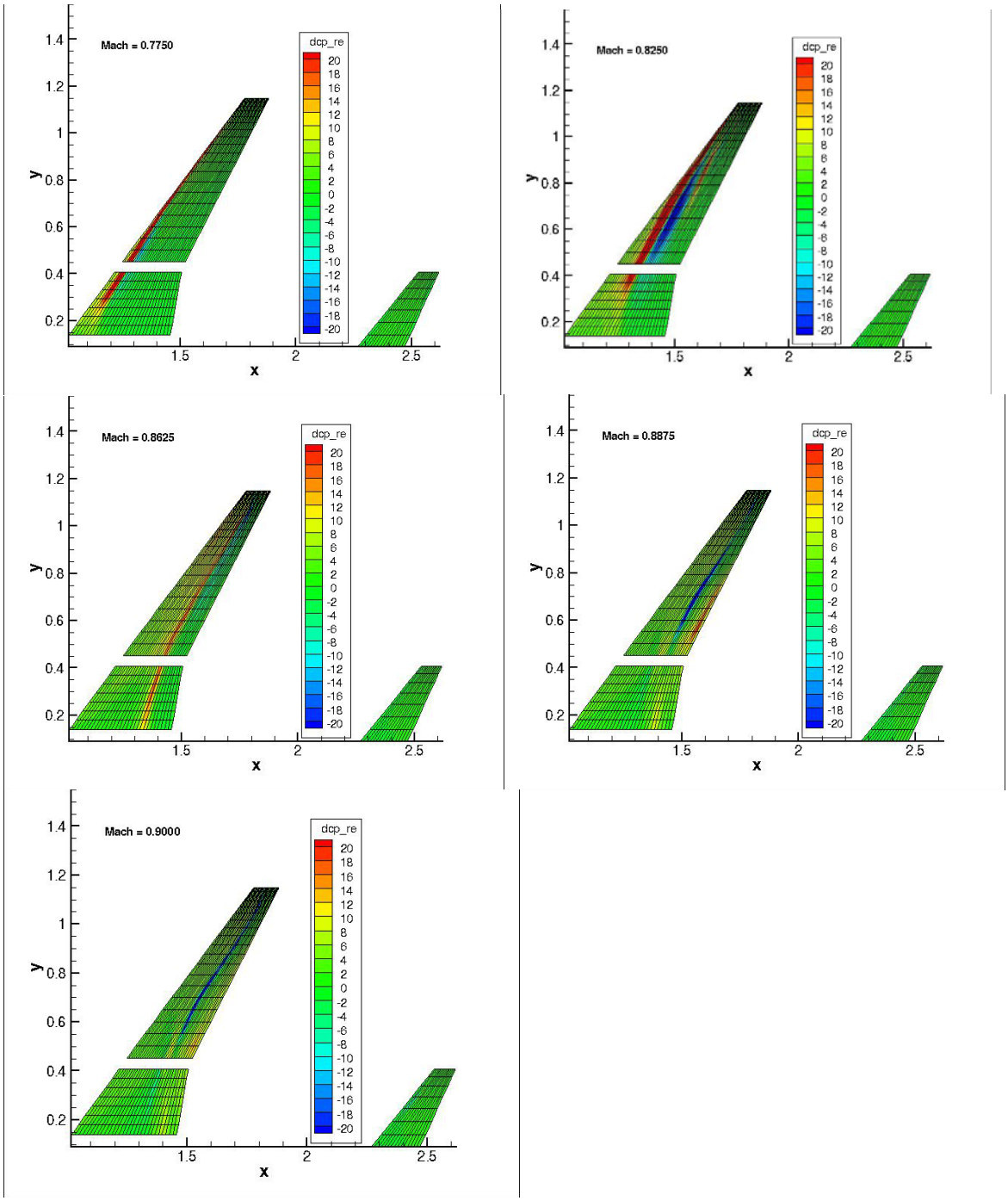

Figure 12: Quasi-steady pressure distribution Δcp/Δα for DPW4 aircraft model mapped on the DLM grid, with varying Mach numbers Ma=0.775, 0.825,0.8625, 0.8875, 0.900, mean flow with CL=0.50, obtained by TAU RANS simulations with Spalart-Almaras turbulence model

Looking closer to unsteady CFD this effect has been observed in windtunnel tests too, for example in the LANN wing test cases CT5 and CT9, see fig.1. In that case the change to inverse shock motion was caused by an increase of the mean AoA, while for the DPW4 model the change is shown by an increase of Mach number. Figure 13 depicts the chordwise unsteady pressure distribution from TAU simulations for two spanwise wing stations of DPW4. For the lower Mach number Ma = 0.8625 the shock peak exhibits the regular behaviour in both real and imaginary parts, while the sign switches for Ma = 0.8875.

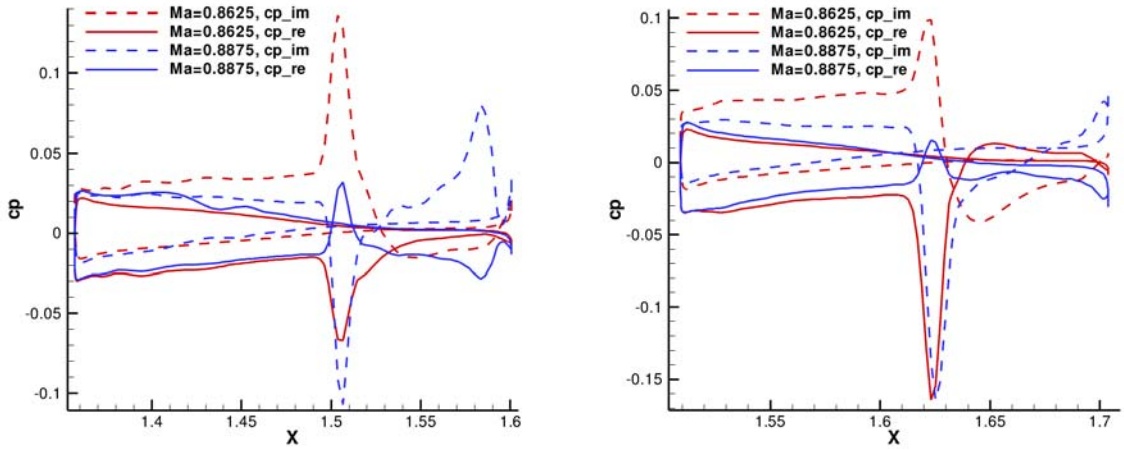

Figure 13: Regular and inverse shock motion for the DPW4, unsteady pressure distribution $\Delta cp/\Delta\alpha$ on upper and lower surface at y=600 mm (left) and y=800 mm (right) spanwise wing stations. Rigid pitching at $\omega^* = 0.25$,

4 FLUTTER BOUNDARY

The flutter boundary was computed by solving an Eigenvalue problem using generalised airloads, which were obtained from pure DLM aerodynamics and from DLM aerodynamics corrected in the above described way using synthetic modes. Results presented herein were obtained by adopting only one single synthetic mode, namely pure rigid pitching, 4 transonic Mach numbers and 4 reduced frequencies.
The DLM grid comprises 1048 surface boxes, 840 of them on the wing. Pressure corrections based on URANS simulations have been introduced only for the wing, because the flow on the tail and fuselage remains subsonic in all cases. Figure 14 depicts the DLM grid.

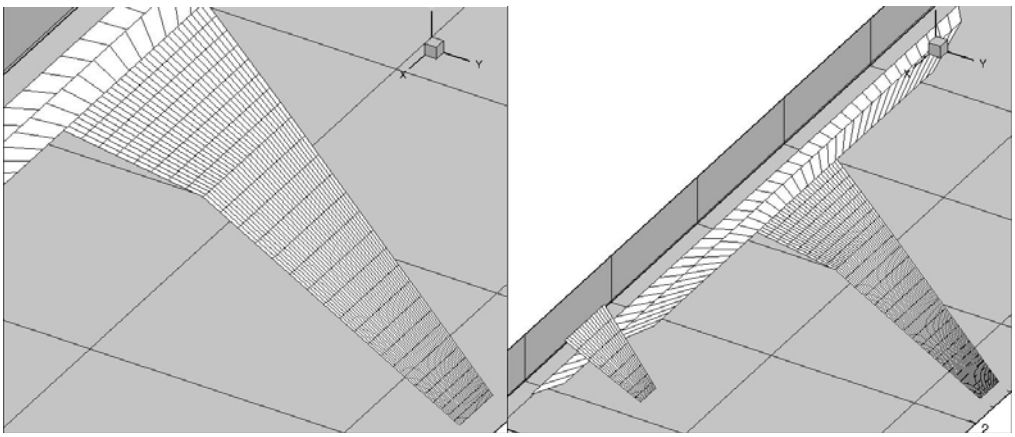

Figure 14: Aerodynamic DLM grid

The correction factors $F_{s,n}$ defined in equation (8) are depicted for the synthetic mode *s=1* (rigid pitching) in figure 15. It shows that the magnitude of *F* increases with increasing Mach number, which is shown by the green, yellow and red colours in the graphs. Similarly figures 16 and 17 show the change of *F* with reduced frequency. While the magnitude decreases, the phase shift increases with reduced frequency on the wing.

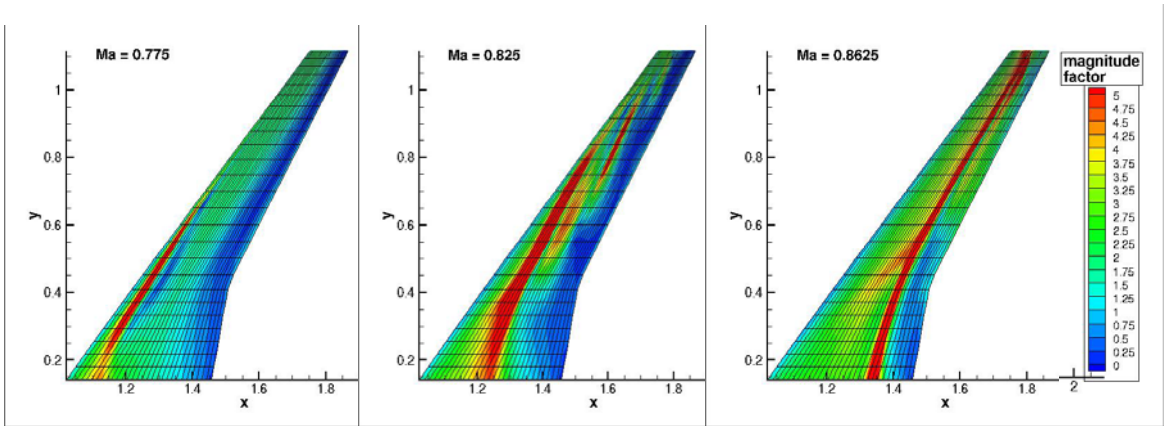

Figure 15: Correction factor for different Mach numbers, 1st synthetic mode, ω* = 0.15

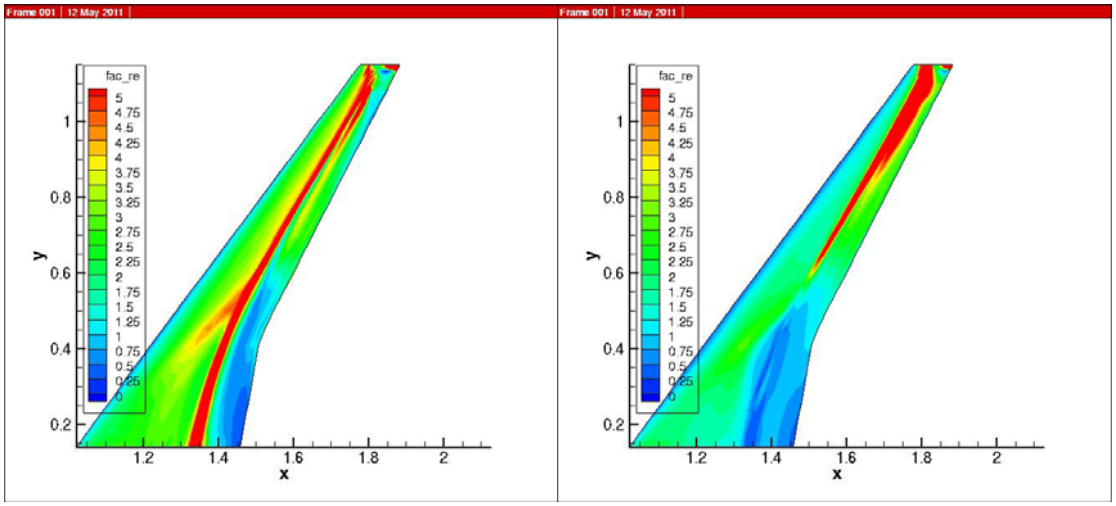

Figure 16: Magnitude of correction factor, 1st synthetic mode, ω* = 0.15 and 1.00

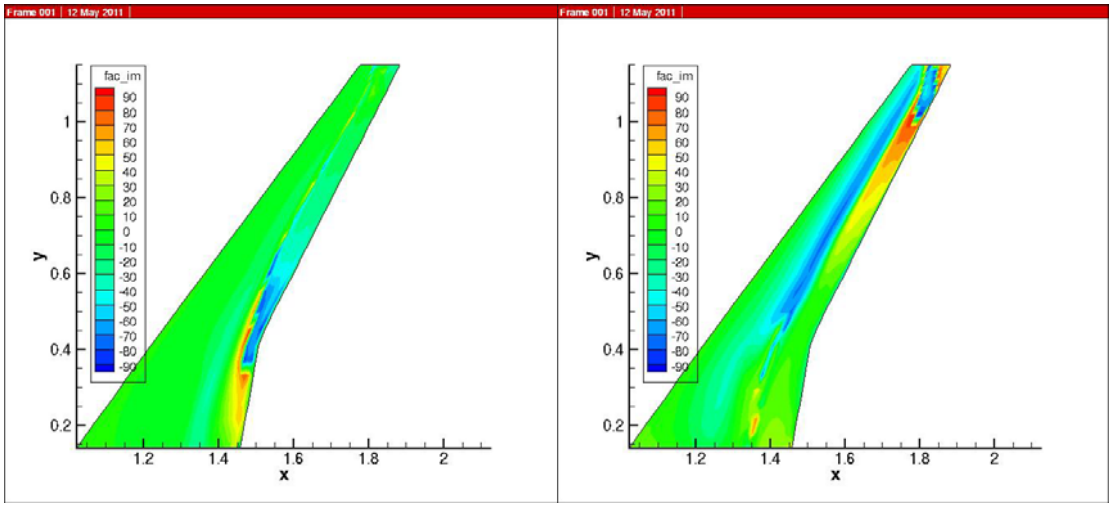

Figure 17: Phase angle of correction factor, 1st synthetic mode, ω* = 0.15 and 1.00

The obtained flutter boundary for the DPW4 model is depicted in figure 18 in form of critical total pressure p_t of the windtunnel as a function of Mach number. The first two eigenmodes

(first bending mode and first torsion mode) couple at a frequency of approximately 30 Hz and cause flutter at p_t between 0.5 and 0.7 bar. The transonic dip behaviour is significant even for the low number of available Mach number values. As the ROM data set currently includes only one synthetic mode, it has to be investigated, how the dip changes when more synthetic modes are included.

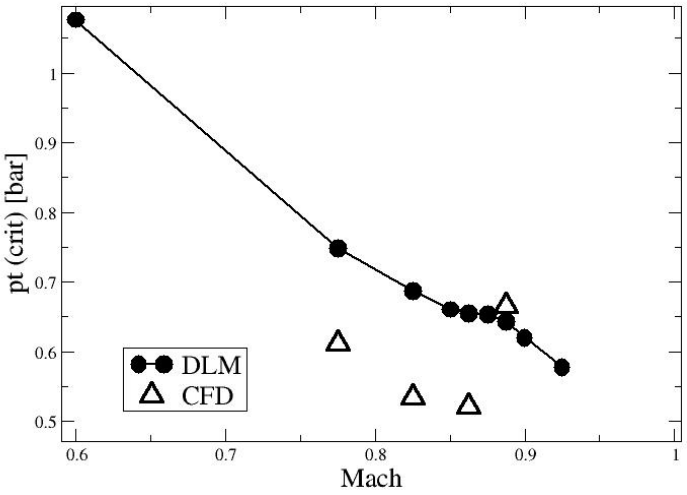

Figure 18: Flutter boundary of the DPW4 model

5 CONCLUSIONS AND OUTLOOK

The configuration of a new numerical flutter model, which is significant for a modern transport aircraft, has been defined and a transonic flutter boundary has been computed with a reduced order model, which uses a CFD data base for the correction of a DLM based flutter process. The model exhibits a clear transonic dip behaviour, the minimum of the dip being close to Mach number of starting flow separation. Separation and corresponding inverse shock motion play a dominant role for the dip. It was demonstrated that the steady CFD simulation results clearly correspond with the dip behaviour too. Currently the numerical dynamic model results on a windtunnel model and contains simple beam-like stiffness and mass elements. In a next step a second model will be derived for full aircraft dimensions and with a more complex finite element model. In a third step, wing engine nacelles and pylons will be added. This will further increase the complexity of the structure and thus increase the demands on CFD based ROMs. DLR will successively extend the ROM data set to more synthetic modes, more Mach numbers and more mass cases.

We would like to propose these models for a specific workshop on the topic "Validation of aeroelastic ROMs for complex applications" and will provide interested partners with the necessary data. The objective of this workshop will be the assessment of different flutter prediction processes and the effort to increase accuracy as well as numerical effort of different aeroelastic ROMs.

6 REFERENCES

[1] Zwaan, ,LANN Wing, Pitching Oscillation, in AGARD Report no. 702, Compendium of Unsteady Aerodynamic Measurements - Addendum, London, August 1982.

[2] Dietz, G., Schewe, G., Kießling, F., Sinapius, M, Limit-cycle-oscillation experiments at a transport aircraft wing model", International Forum of Aeroelasticity and Structure Dynamics (IFASD) 2003, Amsterdam, The Netherland, 4-6, June 2003.

[3] Ballmann, J., Boucke, A., Dickopp C., and Reimer, L. Results of Dynamic Experiments in the HIRENASD Project and Analysis of Observed Unsteady Processes, IFASD-2009-103, International Forum on Aeroelasticity and Structural Dynamics, Seattle, June 21-25, 2009.

[4] Neumann, J. & Ritter, M. Steady and Unsteady Aeroelastic Simulations of the HIRENASD Wind Tunnel Experiment. In Proc. Int. Forum Aeroelast. Struct. Dyn., Seattle, WA, USA, Paper 2009-132 (2009).

[5] Yates, J.C. AGARD Standard Aeroelastic Configurations for Dynamic Response. IWing 445.6. AGARD R765, July 1988.

[6] Goland wing: Beran, P. S., Khot, N. S., Eastep, F. E., Snyder, R. D., and Zweber, J. V., Numerical analysis of store–induced limit–cycle oscillation, Journal of Aircraft, Vol. 41, No. 6, 2004, pp. 1315–1326.

[7] MDO wing, P. Girodoux-Lavigne, J.P. Grisval, S. Guillemot, M. Henshaw, A.Karlsson, V. Selmin, J. Smith, E.Teupootahiti and B. Winzell: Comparison of static and dynamic fluid-structure interaction solutions in the case of a highly flexible modern transport aircraft wing. Journal of Aerospace Science and Technology, 7:121-133, 2003.

[8] Voß, R., Hippe, C., Computation of the flutter boundary of the NLR7301 airfoil in the transonic range, STAB Symposium 2005.

[9] Neumann, J., Nitzsche, J., Voß, R., Aeroelastic Analysis by Coupled Non-Linear Time Domain Simulation. In: Proceedings - AVT-154 Specialists Meeting on Advanced Methods in Aeroelasticity . AVT-154 Specialists Meeting on Advanced Methods in Aeroelasticity , Loen, Norway (2008).

[10] Persoon, A.J., Horsten, J.J., Meijer, J.J., Measurement of transonic dips in the flutter boundaries of a supercritical wing in a wind tunnel, Journal of Aircraft, Vol. 21, No. 11, pp. 906-912, 1984.

[11] Zingel, H. Measurement of steady and unsteady airloads on a stiffness scaled model of modern transport aircraft wing. In Proc. Int. Forum on Aeroelast. Struct. Dynam. DGLR 91-06, 120–131 (1991).

[12] Edwards, John W., Schuster, David M., Spain, Charles V., Keller, Donald F., and Moses, Robert W. MAVRIC Flutter Model Transonic Limit Cycle Oscillation Test, AIAA 2001-1291, Presented at the AIAA/ASME/ASCE/AHS/ASC Structures, Structural Dynamics and Materials Conference, Seattle, WA, April 16-19, 2001.

[13] Albano, E. & Rodden, W. P. A Doublet-Lattice Method for Calculating Lift Distributions on Oscillating Surfaces in Subsonic Flows. AIAA Journal 7 (1969).

[14] Edwards, John W., Transonic Shock Oscillations and Wing Flutter Calculated with an Interactive Boundary Layer Coupling Method, NASA-TM-110284, NASA Langley Research Center (Hampton, VA United States), Aug 01, 1996.

[15] R. Voss, Numerical Simulations of Limit Cycle Oscillations in Transonic Airfoil Flow with Mild Separation, Proceedings of CEAS/AIAA/AIAE International Forum on Aeroelasticity and Structural Dynamics (IFASD), Madrid/Spain, June 5-7 2001, paper 048.

[16] Henke, H. H., Progress of the Viscous-Coupled 3D Euler Method EUVISC and Its Aeroelastic Application, International Forum of Aeroelasticity and Structure Dynamics (IFASD) 2003, Amsterdam, The Netherland, 4-6, June 2003.

[17] Widhalm, M., Dwight, R. P., Thormann, R. & Hübner, A. Efficient computation of dynamic stability data with a linearised frequency domain solver. In Proc. 5th Europ. Conf. Comp. Fluid Dyn. ECCOMAS-CFD, Lisbon, Portugal, June 14-17, 2010 (2010).

[18] R. Voss, G. Brendes: Separation, Proceedings of CEAS/AIAA/AIAE International Forum on Aeroelasticity and Structural Dynamics (IFASD), Madrid/Spain, June 5-7 2001, paper 047.

[19] Thormann, R., Extension of the Subsonic Doublet Lattice Method in Transonic Region using Successive Kernel Expansion. Deutscher Luft- und Raumfahrtkongress 2009, 08.-10. Sep. 2009, Aachen, Germany, 2009.

[20] Palacios, R., Climent, H., Karlsson, A., and Winzell, B., Assessment of strategies for correcting linear unsteady aerodynamics using CFD or experimental results, IFASD 2001–074, 2001.

[21] Timme, S. and Badcock, K. J., Searching for transonic aeroelastic instability using an aerodynamic model hierarchy, AIAA Paper 2010–3048, 2010.

[22] Dowell, E., Edwards, J. & Strganac, T. Nonlinear aeroelasticity. Journal of Aircraft 40, 857–874 (2003).

[23] Brodersen, O., Stürmer, A., Drag prediction of engine-airframe interference effects using unstructured Navier-Stokes calculations, AIAA paper 2001-2414, 2001.

[24] Vassberg, John C., DeHaan, Mark A., Rivers, S. Melissa, and Wahls, Richard A. Development of a Common Research Model for Applied CFD Validation Studies, AIAA Paper 2008-6919, August 2008.

[25] AIAA CFD Drag Prediction Workshop, http://aaac.larc.nasa.gov/tsab/cfdlarc/aiaa-dpw/.

[26] Hall, K. C., Thomas, J. P., and Dowell, E. H., Proper orthogonal decomposition technique for transonic unsteady aerodynamic flows, AIAA Journal , Vol. 38, No. 10, 2000, pp. 1853–1862.

[27] Badcock, K. J. and Woodgate, M. A., Bifurcation prediction of large–order aeroelastic models, AIAAJournal , Vol. 48, No. 6, 2010, pp. 1037–1046.

[28] Gerhold, T., Galle, M., Friedrich, O., Evans, J., Calculation of Complex Three-Dimensional Configurations Employing the DLR-TAU Code. AIAA Paper 97-0167 (1997).

[29] Schwamborn, D., Gerhold, T., Heinrich, R., The DLR-TAU Code : Recent Applications in Research and Industry. Proceedings of the European Conference on Computational Fluid Dynamics – ECCOMAS CFD 2006, Nordwijk, The Netherlands (2006). Available at : http://proceedings.fyper.com/eccomascfd2006/documents/619.pdf.

[30] Spalart, P. R. & Allmaras, S. R. A one-equation turbulence model for aerodynamic flows. AIAA-Paper 92-0439 5–21 (1992).